Electrocatalytic hydrogen evolution in neutral pH solutions: dual phase synergy

Xiaohong Xie,[†] Miao Song,[†] Luguang Wang,[‡] Mark H. Engelhard,[†] Langli Luo,[†] Andrew Miller,[‡] Yayun Zhang,[§] Lei Du,[†] Huilin Pan,[†] Zimin Nie,[†] Yuanyuan Chu,[†] Luis Estevez,[†] Zidong Wei,[#] Hong Liu,[‡] Chongmin Wang,[†] Dongsheng Li,[†] and Yuyan Shao[†]*

- † Pacific Northwest National Laboratory, Richland, Washington 99352, United States
- [‡] Department of Biological and Ecological Engineering, Oregon State University, Corvallis, 97331, United States
- [#] Chongqing Key Laboratory of Chemical Process for Clean Energy and Resource Utilization, School of Chemistry and Chemical Engineering, Chongqing University, Chongqing 400044, China
- § Bioproducts, Sciences and Engineering Laboratory, Department of Biological Systems Engineering, Washington State University, Richland, Washington 99352, United States

Supporting Information

ABSTRACT: Electrolysis in neutral pH solutions (e.g., wastewater, seawater) presents a transformative way for environmentally friendly, cost-effective hydrogen production. However, one of the biggest challenges is the lack of active, robust hydrogen evolution reaction (HER) catalysts. Herein we present a novel catalyst with dual active sites of MoP₂ and MoP which function synergistically to promote HER in neutral pH solutions. In a real microbial electrolysis cell (MEC) which uses neutral pH wastewater as feedstock, the new catalyst delivers an average HER current density of 157 A m⁻²Cathode-Surface-Area, higher than Pt/C catalyst (145 A m⁻²Cathode-Surface-Area), ~5 times higher than the state-of-art platinum group metal (PGM)-free catalysts in MECs. The new catalyst also outperforms Pt/C in natural seawater with ~10% higher and more stable HER current density. The fundamental reason for the enhanced HER performance is identified to be the synergy between MoP₂ and MoP phases, with MoP₂ promoting H₂O dissociation and MoP efficiently converting H_{ad} to H₂.

KEYWORDS: hydrogen evolution reaction, neutral pH solution, molybdenum phosphide, electrocatalyst, water splitting

Hydrogen has attracted considerable attention as an abundant energy carrier.1-3 One efficient and sustainable route to generate hydrogen is catalytic hydrogen evolution reaction (HER) from water. 4 Platinum-group-metals (PGM) are known to efficiently catalyze HER. However, for practical application, it has been significantly limited by their scarcity and high cost. PGM-free HER catalysts based on inexpensive transition metals, including nitrides, carbides, borides and chalcogenides have been explored in the past few years. 6-9 However, most of such catalysts only function well in acidic or alkaline solutions, but underperform in neutral pH solutions.10 Generating H₂ from mild neutral pH solutions (e.g., wastewater, seawater) has shown advantages of being environmentally friendly, sustainable, and cost-effective by enabling new, low cost electrocatalysts and feedstocks." It may also provide an efficient way for environmental cleanup, for example, H2 production using a microbial electrolysis cell (MEC) cleans wastewater.12-14 HER catalysts for neutral solutions, which has been less explored, is highly attractive but remains a grand challenge.

Previous studies indicated that H_2O dissociation ($H_2O + e^- + M \rightarrow M-H_{ad} + OH^-$, where M stands for metal and H_{ad} is H adsorbates) and H_{ad} recombination ($H_2O + M-H_{ad} + e^- \rightarrow$

 $M + H_2 + OH^-$ or $H_{ad} \rightarrow H_2$) are the key steps in neutral pH HER. ¹⁵ Those reaction steps fundamentally depend on how H_2O , OH and H bond to the catalysts' surface. ¹⁶ A plausible way to accelerate the kinetics of H_2O dissociation is to use "promoter" such as metal hydroxides/oxides with the function to cleave the HO-H bond. ¹⁷⁻¹⁹ Limitations in the catalytic activities of most of the promoters lies in the fact that they are generally poor at converting H_{ad} into H_2 . ²⁰⁻²² They have relied on the use of active H_{ad} recombination catalysts such as Pt that exhibits an optimum H_{ad} binding energy. ²³⁻²⁴ These pioneering understandings hold the promise that the sluggish kinetics of neutral pH HER might be improved if rational design of robust bifunctional systems is achieved and the synergy between "promoters" and PGM-free catalysts is exploited.

Molybdenum phosphides (MoP_x) have been extensively investigated as a versatile functional catalyst for various reactions, including HER and hydrodesulphurization catalysis. $^{25\text{-}27}$ It has been proven that MoP_x exhibits weak electron delocalization effect between Mo and P because more electronegative P can drew electrons from Mo. 28 This suggests that to increase the atomic percentage of P is expected to improve the strength of "Mo $^{\delta+}$ -P $^{\delta-}$ " bond and thus to create

a robust bifunctional system similar to " $M^{2+\delta}O^{\delta}(OH)_{2-\delta}/Pt$ " for efficient H₂O chemisorption and dissociation.¹⁷ Moreover, recent density functional theory (DFT) calculations indicate that MoP_x is a good H_{ad}-delivery system which could potentially modify the catalytic properties of the active Mo sites,28 pointing toward a possibility for further optimization in H_{ad} recombination. However, the role of Mo and P, and the effect of their interaction on its HER catalytic performance remain unclear, particularly in neutral pH solutions, which stands as a critical obstacle for understanding the structure-property relationship for better HER catalyst development. A new synthesis approach is also needed for the preparation of MoP_x because conventional approaches through calcining mixed Mo and P precursors generally involves excessive coarsening of crystallites, resulting in poor control of MoP_x structure and morphology.²⁹⁻³⁰

Herein we report a "dual active sites" MoP₂/MoP nanocomposite catalyst to boost the overall HER process in neutral pH solutions: MoP₂ phase with a high contrast between the electrostatic affinity of Mo^{δ_+} to -OH and P^{δ_-} to -H to accelerate H₂O dissociation, and MoP phase with optimum exposure of Mo atoms to provide active sites for Had recombination. The bifunctional MoP₂/MoP composite is formed from a phase-controlled phosphidation of Mo-rich polyoxometalate (rPOM) nanoclusters at a certain temperature of 700 °C (this catalyst is designated as MoP700). MoP700 exhibits exceptional HER activity and outstanding stability in neutral pH solutions, better than Pt/C in a real MEC device and for seawater splitting. Our theoretical calculation confirms that the enhanced HER activity of MoP700 in neutral pH solutions comes from the synergy of MoP₂ and MoP for H₂O chemisorption/activation and H₂O/H binding.

The synthesis of the MoP700 catalyst involves two steps. In the first step, pristine POM was used to prepare nanostructured rPOM (reduced POM) through a reductive route (see Methods). POMs are metal oxide clusters of group 5/6 elements that can accept/release electrons without destructing their nanostructures.31 The reduction technique transforms bulky POM into discrete rPOM nanoclusters (~5 nm, Figure S1). In the second step, the uniformly mixed rPOM and NaH₂PO₂ precursors (mass ratio of rPOM/NaH₂PO₂ is 1/5.8) are preheated at 240-300 °C (0.5 °C mim⁻¹) for 2 hours in a tube furnace under flowing Ar; then the furnace temperature was increased to 700 °C (5 °C mim⁻¹) which transformed rPOM to a mixture of MoP/MoP₂ crystalline phases through a phosphidation process by PH3 which is produced by in situ thermal decomposition of NaH₂PO₂ (Figure S2). For comparison, pure MoP₂, Mo₃P catalysts were also prepared by varying the mass ratio of Mo/P precursors, while MoP was obtained by further heating the MoP700 catalyst in Ar environment at 750 °C.

Figure 1a presents an overall transmission electron microscopy (TEM) image of the synthesized MoP700 with nanoparticle size in the range of 8-30 nm. High-resolution TEM (HRTEM) image (Figure 1b) further reveals a crystalline nature and a MoP2/MoP heterostructure of the catalyst (Figure S3). The imaged lattice fringes with interplane spacings of 0.21 nm correspond to MoP (101) plane (Figure 1c) and the enlarged d-spacings of 0.56 nm is for MoP2 (020) plane

(Figure 1d). HRTEM images of MoP700 also show the distribution of Mo and P with MoP and MoP2 both exhibiting Mo-terminated surfaces (Figure S4). The crystal structure difference of MoP and MoP2 phases is clearly visible from their Fast-Fourier-Transforms (FFT) in inset Figures 1c and 1d, respectively. Qualitative energy dispersive X-ray spectroscopy (SEM-EDS) analysis confirms the elemental compositions of selected area of MoP and MoP2, which are consistent with their chemical formulas, ~47.5:52.5 (~1:1) and 36.8:63.2 (~1:2) for MoP and MoP2, respectively (Figure 2a). Moreover, a Mo/P ratio of ~1.5 in bulk MoP700 was derived from the overall SEM-EDS elemental maps, suggesting the MoP2/MoP ratio in MoP700 is ~1:1. X-ray diffraction (XRD) patterns of catalysts confirms the co-existence of MoP and MoP2 phases in MoP700 (Figure 2b).

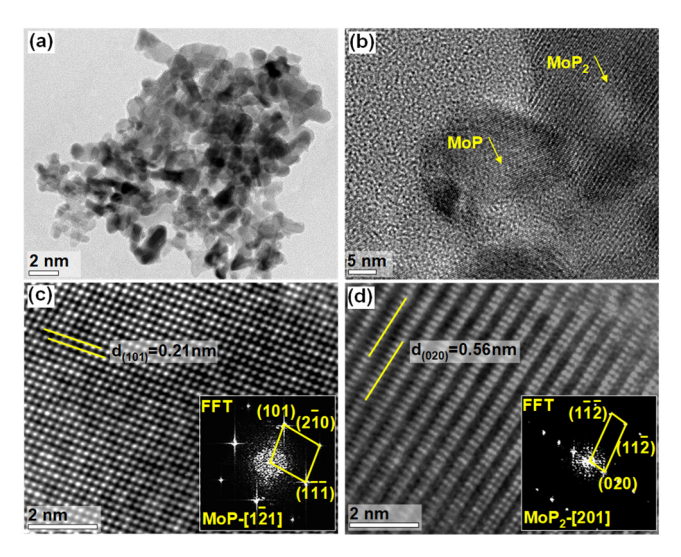


Figure 1. (a) Overall TEM image of the MoP700 catalyst, (b) HRTEM image of MoP700 revealing a MoP and MoP₂ heterostructure. (c-d) HRTEM images of MoP700 to show the structure difference of MoP (c) and MoP₂ (d). Inset (c) and (d) are Fast Fourier transforms (FFT) of the MoP and MoP₂, respectively.

The surface chemical states of MoP700 was investigated by X-ray photoelectron spectroscopy (XPS). The Mo 3d region of MoP700 show binding energies of 232.63 and 228.81 eV indicative of $Mo^{\delta+}$ (o < $\delta \le 4$) species generally assigned to Mo in MoP_x, and the rest of the Mo doublets at 236.35 eV and 233.39 eV can be ascribed to high oxidation state of Mo (MoO_x) (Figure 2c).32 The P 2p spectrum of MoP700 exhibits two major peak regions (Figure 2d), with one centred at binding energies of 130.45 eV and 129.65 eV, which can be attributed to P bonded to Mo in the form of a phosphide,33 and the other peaks at 134.87 and 133.5 eV characteristic of metaphosphate. The existence of oxidized Mo and P can be attributed to catalyst surface oxidation under air condition as often observed for metal phosphides.³⁴⁻³⁶ Moreover, the binding energies for Mo and P of catalysts are in the orders $Mo^{\circ} < MoP < MoP_{700} < MoP_{2}, P^{\circ} > MoP > MoP_{700} > MoP_{2},$ respectively, indicating that Mo and P in MoP700 bear enhanced positive (δ^+) and negative (δ^-) charges, respectively. This result points to the formation of strong "Mo $^{\delta+}$ -P $^{\delta-}$ " networks in MoP700, which could potentially mimics the catalytic behaviour of " $M^{2+\delta}O^{\delta}(OH)_{2-\delta}/Pt$ " or " $Au/Pt-S_{ad}^{\delta-n}$ " systems for efficient H_2O dissociation, 17, 23, 37 and promotes the overall HER on the MoP_2/MoP heterostructured catalyst.

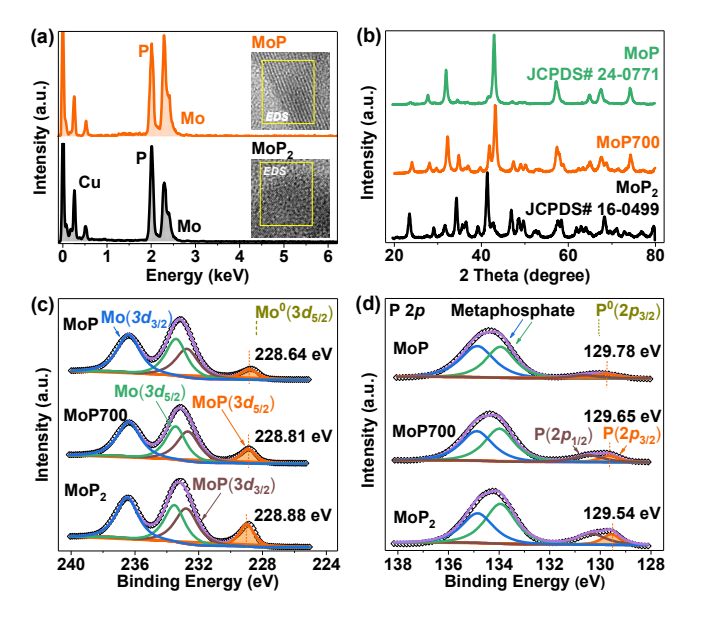


Figure 2. (a) SEM-EDS analysis of MoP700. (b) XRD pattern of MoP700 in comparison with MoP₂ and MoP. (c-d) high resolution Mo 3d (c) and P 2p (d) XPS spectra for MoP700, MoP₂ and MoP.

HER electrocatalytic activity of catalysts were first assessed in 1.0 M H₂-purged phosphate buffer solution (PBS, pH 7.4) using a three-electrode cell. Figure 3a-b shows the HER polarization curves and corresponding Tafel plots of MoP700 compared with those of MoP₂, MoP, Mo₃P and 20 wt% Pt/C (ETE-K). MoP700 exhibits a low onset overpotential (n) of 75 mV, slightly higher than Pt/C (45 mV). The η at current density (j) of 10 mA cm⁻²geometric is 196 mV for MoP700, close to 181 mV for Pt/C and significantly lower than 276, 327 and 491 mV for MoP₂, MoP and Mo₃P, respectively. Those η values on MoP700 are smaller than most PGM-free HER catalysts reported to date, placing its catalytic activity among the best in neutral pH HER (Table S1). From the extrapolation of the liner region of a plot of η versus log (j), we obtained Tafel slope values of 79, 97, 87, 153 and 107 mV dec-1 for MoP₇00, MoP₂, MoP, Mo₃P and Pt/C, respectively. The smallest slope of MoP700 indicates a two-electron transfer process following a "Volmer-Tafel" mechanism of 2Hads adsorption and H₂ evolution occurring on MoP700's surface, which also demonstrates favorable H2O adsorption/dissociation and Had recombination kinetics on MoP700.38-39

Electrochemical impedance spectroscopy (EIS) was used to study the electrode kinetics of the catalysts under the HER mode. The charge transfer resistance (R_{ct}) tells the kinetics of electrocatalysis on electrode, and a lower R_{ct} value corresponds to a faster reaction rate.⁴⁰⁻⁴¹ It is found that the R_{ct} values of the electrodes show similar tendency to that previously observed in HER tests, with MoP700 exhibiting the smallest R_{ct} of 93 ohms(Figure 3c and Figure S5). This result indicates that the high conductivity of MoP700 (Figure S6) and the fast charge transport at the MoP700/electrolyte interface are the key factors contributing to the superior neutral pH HER kinetics of the MoP700 electrode.

The stability is also critical for electrocatalysts in an energy conversion system. The HER stability of the MoP700 catalyst was investigated using a dynamic potential protocol by cycling electrode potential between -0.45 and 0.15 V versus RHE for 4,000 cycles at scan rate of 50 mV s⁻¹. This type of accelerated stability test is developed to represents the cycling expected for real electrolysis devices. Continuous gas bubbling was observed on the MoP700 electrode throughout the stability test (Video S1). As shown in Figure 3d, the η of MoP700 electrode at 10 mA cm⁻²geometric increased only by ~10 mV after the stability cycling, demonstrating a high catalytic stability of MoP700. In addition, as given in Figure <u>S7-8</u>, inspection of the morphology and oxidation states of Mo and P after the stability test reveals no difference compared to the one before the test, affirming the excellent stability of MoP700.

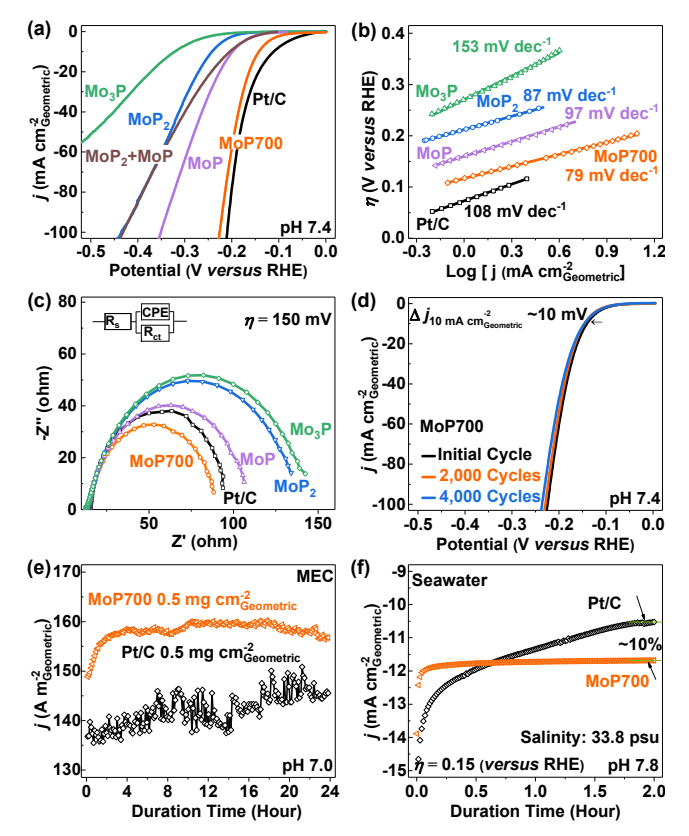


Figure 3. (a) Polarization curves (iR-free) for HER on different catalysts in H₂-purged 1.0 M PBS (pH 7.4); 1600 rpm; 5 mV s⁻¹; (b) Tafel plots derived from the HER curves in (a). (c) Electrochemical impedance spectra of different electrodes at η of -150 mV; inset: Equivalent circuit used for data analyses; R_s and R_{ct} are the ohmic and charge transfer resistance, respectively. (d) Cycling stability of MoP700 (HER polarization curves before and after the stability tests). All electrochemical data were obtained after cyclic-potential activation. (e) Current generation for Pt/C and MoP700 cathodes at electrode loading of 0.5 mg cm⁻² (Anode: 10 cm² carbon cloth with enriched electrochemically active bacteria; Cathode: 1.0 cm2 catalysts loaded carbon cloth; 200 mM phosphate buffer (pH 7.0) with 75 mM sodium acetate; voltage: 1.0 V). (f) HER on MoP700 and Pt/C catalysts in seawater (pH 7.8, salinity 33.8 psu, no iR-correction); scan rate: 5 mV s⁻¹; rotation rate: 1600 rpm.

We further evaluated MoP700 for real HER application in an MEC device. As shown in <u>Figure 3e</u>, at the same catalyst

П

loading of 0.5 mg cm⁻²Cathode, the MEC with the MoP700 catalyst can generates a maximum current density of 157 A m⁻²Cathode-Surface-Area, higher than that with the Pt/C catalyst (145 A m⁻²Cathode-Surface-Area). The exceptional high current density achieved here demonstrates that the cathode with MoP700 is capable of generating H₂ ~5 times faster than previously reported MECs (Table S2). The MEC with MoP700 cathode also showed high catalytic stability during the MEC operation. MoP700 also has high and stable catalytic HER activity in natural seawater (Figure 3f). Overall, the outstanding HER performance of the MoP700 catalyst show a great potential for real application in H₂ production in neutral pH solution systems.

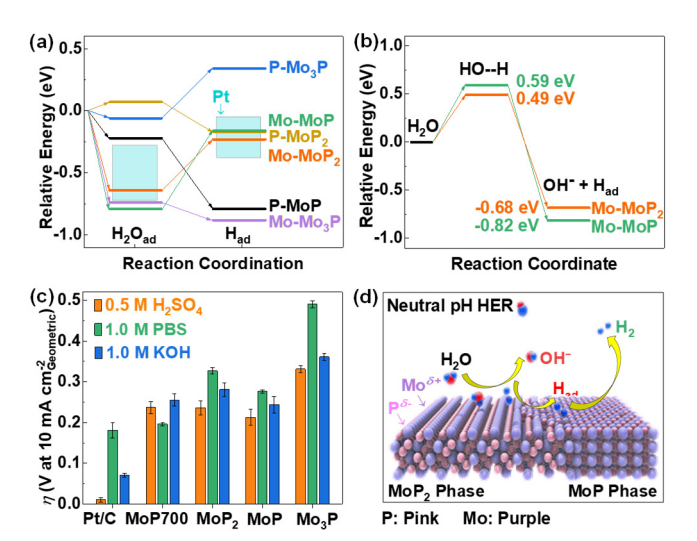


Figure 4. (a) Calculated binding energy of H₂O and H adsorption on MoP₂, MoP and Mo₃P, Mo- and P-terminated surfaces. (b) Calculated kinetic reaction energy barrier for H₂O dissociation on Mo-MoP and Mo-MoP₂ surfaces. (c) Comparison between catalytic activity of the HER in acidic, neutral and basic solutions for MoP₇oo, MoP₂, MoP, Mo₃P and Pt/C. Error bars are s.d. of at least 5 sets of experimental repeats. (d) Schematic representation of neutral pH HER on MoP₇oo.

We hypothesize that the excellent HER performance of the MoP700 catalyst is the direct outcome of its special heterojunction-like MoP2/MoP structure imparted by the unique chemical synthesis approach. To prove this hypothesis, we compared the intrinsic activity of catalysts by normalizing the measured current densities to their electrochemical active surface area (ECSA). MoP700 exhibits a η of 201 mV at j of 0.3 mA cm²ESCA, outperformed MoP2, MoP and Mo3P by 115, 89 and 261 mV (Figures S9 and S10), highlights that MoP700 is a highly active neutral pH HER catalyst. In addition, we compared the HER activity of MoP700 and physically mixed MoP2/MoP, with MoP700 is far better than the mixture (Figure 3a). Those results suggested that the catalytic HER reactivity is facilitated by a synergistic effect between MoP2 and MoP.

To understand the origin of the high neutral pH HER catalytic activity of MoP700, we performed DFT calculations. We firstly calculated the binding strength (ΔE_b) of H₂O and H to both Mo- and P-terminated MoP₂, MoP and Mo₃P surfaces (<u>Figure Sn</u>). Generally, neutral pH HER involves H₂O adsorption/activation and H recombination on the surface

of catalyst; so, a strong bonding of H₂O and weak bonding of H to surface is desired. 15, 42 We found that only Mo-MoP₂ surface has superior H₂O chemisorption property and only Mo-MoP₂ and Mo-MoP surfaces show preferential binding for H (Figure 4a) in comparing with the ΔE_b of H₂O on Pt,⁴³ ⁴⁶ indicating those two surfaces are the catalytic active surfaces for the neutral pH HER, which agree well with the observed surface structure of MoP700 with Mo-terminated surfaces. We further calculated the kinetic reaction barriers (ΔE_a) for the dissociation of H₂O on Mo-MoP₂ and Mo-MoP surfaces. The ΔE_a for the transition state and final state of H₂O decomposition on Mo-MoP₂ surface were determined to be lower than that on Mo-MoP surface (Figure 4b, Figure S12), suggesting a superior H₂O dissociation capability of Mo-MoP₂ surface. Meanwhile, on Mo-MoP surface, the ΔE_h for H was calculated to be lower than on Mo-MoP₂ surface. This suggests that the H_{ad} produced on Mo-MoP₂ sites could be "delivered" to the nearby Mo-MoP sites to form "H-H" bond more effectively if both Mo-MoP₂ and Mo-MoP₂ surfaces are stay closely together in the catalyst. In MoP700, the MoP2-MoP synergy not only facilitates the H₂O chemisorption/dissociation, but also promotes the H-H bond formation of two adjacent H_{ad} that, finally, recombine into molecular hydrogen (H₂). All of these synergistic effects contribute to the enhanced neutral pH HER activity of MoP700.

Additional catalytic studies were conducted to get further insights into the origin of the high HER activity of MoP700 in PBS. Figure 4c compares the HER catalytic activities (expressed as η values at j of 10 mA cm⁻²_{Geometric}) of MoP₇00, MoP₂, MoP, Mo₃P and Pt/C catalysts in acidic, neutral and basic solutions. For the MoP₂, MoP and Mo₃P catalysts, the HER activity increases in the order acidic > basic > neutral, consistent with the observed trend for Pt/C. However, the HER activity trend for MoP700, neutral > acidic > basic, is inverse to that observed on the other electrodes, indicating that the HER on MoP700 is controlled by the activity of the MoP₂/MoP coexists structure/surface. We hypothesize the neutral pH HER mechanism on MoP700 surface as shown in Figure 4d. Previous calculation of the P-terminated surface on MoP_x implies that the binding of H⁺ on P is unfavorable when the H coverage is high.²⁸ The result is that P could "poisons" the active sites for H_{ad} formation/recombination. On the other hand, in basic solution, because H₂O dissociation is kinetically facile on MoP700 while the HER activity is neutral < basic, therefore, desorption of OHad to refresh the catalysts' surface might be the key step for HER. That is, the OH⁻ from the electrolyte/H₂O could either occupy or prevent the desorption of OH_{ad} from the catalytic active sites for further H₂O chemisorption/dissociation on MoP700, causing inefficient release of OH_{ad} and then deactivating of the catalyst. The roughly equivalent HER activity on MoP700 in acidic and basic electrolytes might be related to the similar "blocking effect" of excess H⁺ or OH⁻ on the performance of MoP700 in HER. At this point, keeping in mind that HER of MoP700 in neutral solution is almost independent of H⁺/OH⁻ and the activity is MoP₇oo > MoP > MoP₂, we suggest that the surface "MoP₂/MoP" enabled fast H₂O dissociation step is the key for the high catalytic activity.

In conclusion, nanostructured MoP700 composite catalyst with a MoP/MoP₂ heterostructure has been synthesized by a two-step mix-phosphidation processing method and exhibits outstanding activity and stability for HER in neutral pH solutions, which is even better than Pt/C catalyst in real MEC devices (wastewater as a feedstock) and natural seawater. Based on our experimental and theoretical studies, we propose a synergistic mechanism of between the two phases of MoP₂ and MoP that is responsible for the high neutral HER catalysis activity. This study also provides a new approach to controllable design and synthesis of PGM-free, highly efficient and biocompatible systems which may find applications in other catalysis fields.

METHODS

Synthesis of Pristine POM. 0.01 mol (NH₄)₆Mo₇O₂₄·4H₂O (\geq 99%) and 0.006 mol H₃PO₄ (85%) were dissolved in 200 mL DI water (18.2 M Ω cm) under vigorous stirring. Then 8 mL of concentrated HNO₃ (70%) was dropwise added into the above mixture and kept at 80 °C for 1 day. The resulting yellow colloidal product ((NH₄)₃PMo₁₂O₄₀) was centrifuged and washed with 1.0% HNO₃ solution and vacuum dried at 80 °C for 24 hours.⁴⁷

Synthesis of rPOM (Reduced-POM). 5.0 g of POM was dispersed in 50 mL of DI water. Then 0.25 g of NaBH₄ was added to the above dispersion under stirring: as soon as the reduction of the POM occurred, gas evolution (NH₄⁺ + H⁻ \rightarrow NH₃ + H₂) took place and the solution color changed to dark-blue. After stirred for 10 hours to allow the complete reaction of the POM, rPOM nanoclusters-containing solution was centrifuged at a speed of 10,000 rpm for 1 hour to precipitate the impurities, and then, the resulting solution was separated and dried in a freeze-dryer to obtain rPOM.

Synthesis of MoP700 Catalyst. 1.0 g of rPOM powder was fine-grained mixed with 5.8 g of NaH₂PO₂·H₂O (P:Mo ~1:8). The mixture was preheated at 240-300 °C (0.5 °C min⁻¹) for 2 hours (0.5 °C min⁻¹) and then calcined at 700 °C (5 °C min⁻¹) for 5 hours under flowing Ar. The resulted black-colored product was well grinded and dispersed in 0.5 M HCl solution and kept at 80 °C for 1 hour, then centrifuged, washed with water and ethanol for several times and vacuum dried at 80 °C for overnight. Advantages of this methodology include high reproducibility, avoidance of complicated purification procedures, and easy scale-up of up to gram quantities.

Material Characterization. Scanning/transmission electron microscopy (S/TEM) and high-resolution TEM images were obtained by a FEI Titan system. X-ray diffraction patterns (XRD) were collected using a Philips Xpert X-ray diffractometer in a CuK α tube at λ =1.5418 Å. X-ray photoelectron spectroscopy (XPS) was obtained using a Kratos Axis Ultra DLD spectrometer. All peaks were adjusted based on C1s peak at 284.5 eV as a reference.

Electrochemical Tests. All the electrochemical tests were performed in a standard three-electrode setup using a CHI 66oD electrochemical workstation using an Ag/AgCl reference electrode and graphite-rod as counter electrode. The Ag/AgCl electrode was calibrated in H₂ (99.99%)-saturated

0.5 M H₂SO₄ electrolyte using Pt wire for both the working and counter electrodes to -0.255 V versus the reversible hydrogen electrode ($E_{(RHE)}$ = 0.059 pH + 0.255 V). To prepare working electrode, 5.0 mg of catalyst was mixed with 3980 uL 70% water/isopropyl-alcohol and 20 uL of 5 wt% Nafion solution by sonication for 30 minutes. Subsequently, 40 uL of the catalyst ink was drop-dried onto glassy carbon electrode to cover an area of 0.1962 cm² (catalyst loading: ~0.25 mg cm⁻²). All the potentials reported in this work were converted to RHE and all the HER polarization curves were iRcorrected. AC impedance measurements were conducted in the same configuration when the working electrode was biased at overpotential of 100, 125 and 150 mV versus RHE from 105 Hz to 10-1 Hz with an AC voltage of 5 mV. All the electrochemical data were obtained after electrochemical cyclic potential (CV) activation for 50 cycles (o to 0.6 V versus RHE). All HER polarization curves were collected after electrochemical potential activation for 3 scans (LSV, 0.15 to -0.45 V, versus RHE). CV between -0.45 and 0.15 V (versus RHE) at scan rate of 50 mV s⁻¹ for 4,000 cycles was performed to evaluate the HER stability. All tests were conducted 5 times to avoid any incidental error.

DFT Calculation. DFT calculations were performed by Vienna ab-initio simulation package (VASP) with the projector augmented wave pseudo-potentials to describe the interaction between atomic cores and valence electrons with DFT. The Perdew Burke Ernzerhof (PBE) functional within the generalized gradient approximation (GGA) was used to implement DFT calculation. The MoP, MoP₂, Mo₃P(oo₁) by the Mo and P-terminated slab models were used to simulate the surface properties. The reasonable vacuum layers were set to 15 Å in the z-direction for avoiding interaction between MoP_x planes. A cutoff energy of 400 eV was provided and a 4×4×1 Monkhorst Pack k-point sampling was used for the well converged energy values. Geometry optimizations were pursued until the force on each atom falls below the convergence criterion of 0.02 eV Å-1 and energy was converged within 10⁻⁵ eV. The lowest two layers atoms were fixed, and the other atoms were allowed to move during the geometry optimization in the Mo and P-terminated surface. The differential adsorption energy of H atom can be estimated by using the equation:

$$\Delta E_{ad} = E_{ad/base} - E_{ad} - E_{base}$$

where $E_{\rm ad/base}$, $E_{\rm ad}$, and $E_{\rm base}$ represent the total energy of the adsorbed systems, the isolated H or H₂O, and the base, respectively. The negative ΔE_{ad} demonstrates the energetically favorable interaction between adsorbate and slab surface.

Microbial Electrolysis Cell (MEC) Construction, Inoculation, and Operation. Single chamber MECs were used to compare the performance of MoP700 with Pt/C catalyst. The MECs were made from narrow mouth media bottles sealed with butyl septum topped caps. The total reactor volumes were 320 mL with a liquid volume of 100 mL and a gas volume of 220 mL. The MECs cathode with loadings of 0.5 mg cm $^{-2}$ MoP700 (or Pt/C) were fabricated as follows: (1) desired loading of catalyst was mixed with Nafion (5%) for 10 hours in a ratio of 7 μ L mg $^{-1}$ of catalyst to form a paste; 2) the paste was uniformly pipetted to both sides of the

cathode material; 3) the painted cathode was left to dry out at 25 °C for 1 day. The cathode had a projected surface area of 1 cm². The anode was plain carbon cloth (CC) with a projected surface area of 10 cm². MEC was inoculated by scraping mature biofilm from a previously enriched MEC anode and applying the biofilm on the plain CC anode, and operated sequentially with a medium solution containing 200 mM phosphate buffer, 75 mM sodium acetate and necessary nutrients as reported previously. The applied voltage across the electrodes was fixed at 1.0 V. Temperature was controlled at 32 °C. Current was measured by recording the voltage across a serially connected 1 Ω resistor using a multimeter with a data acquisition system (Keithley). Calculation of current density was performed as described previously. 49

ASSOCIATED CONTENT

Supporting Information.

The Supporting Information is available free of charge on the ACS publications website at DOI: 10.XXX.

Additional Figures and Tables as described in the text.

AUTHOR INFORMATION

Corresponding Author

*E-mail: yuyan.shao@pnnl.gov

Notes

We are filing a patent.

ACKNOWLEDGEMENT

This work was financially supported by the US. Department of Energy's (DOE) Fuel Cell Technology Office. D.S. Li acknowledges the support by the U.S. Department of Energy (DOE), Office of Science, Office of Basic Energy Sciences (BES), Division of Materials Science and Engineering (DMSE) through the Early Career Research Program Award. C.M. Wang thanks the support of the Laboratory Directed Research and Development Program at the US. Pacific Northwest National Laboratory (PNNL). The electron microscopy and XPS analysis were performed at the William R. Wiley Environmental Molecular Sciences Laboratory (EMSL), a national scientific user facility sponsored by the DOE's Office of Biological and Environmental Research and located at PNNL. PNNL is operated by Battelle for the DOE under Contract DE-ACO5-76RLO1830.

REFERENCES

- 1 Chu S, Majumdar A. Opportunities and challenges for a sustainable energy future. Nature. 2012;488(7411):294-303.
- 2 Hosseini SE, Wahid MA. Hydrogen production from renewable and sustainable energy resources: Promising green energy carrier for clean development. Renew Sust Energ Rev. 2016;57:850-66.
- 3 Jain IP. Hydrogen the fuel for 21st century. Int J Hydrogen Energ. 2009;34(17):7368-78.
- 4 Dincer I, Acar C. Review and evaluation of hydrogen production methods for better sustainability. International Journal of Hydrogen Energy. 2015;40(34):11094-111.
- 5 McCrory CC, Jung S, Ferrer IM, Chatman SM, Peters JC, Jaramillo TF. Benchmarking hydrogen evolving reaction and oxygen evolving reaction electrocatalysts for solar water splitting devices. J Am Chem Soc. 2015;137(13):4347-57.

- 6 Kong D, Cha JJ, Wang H, Lee HR, Cui Y. First-row transition metal dichalcogenide catalysts for hydrogen evolution reaction. Energy & Environmental Science. 2013;6(12).
- 7 Chen WF, Sasaki K, Ma C, Frenkel AI, Marinkovic N, Muckerman JT, et al. Hydrogen-evolution catalysts based on non-noble metal nickel-molybdenum nitride nanosheets. Angew Chem Int Ed Engl. 2012;51(25):6131-5.
- 8 Wu HB, Xia BY, Yu L, Yu XY, Lou XW. Porous molybdenum carbide nano-octahedrons synthesized via confined carburization in metal-organic frameworks for efficient hydrogen production. Nat Commun. 2015;6:6512.
- 9 Gong QF, Cheng L, Liu CH, Zhang M, Feng QL, Ye HL, et al. Ultrathin MoS2(1-x)Se2x Alloy Nanoflakes For Electrocatalytic Hydrogen Evolution Reaction. Acs Catalysis. 2015;5(4):2213-9.
- 10 Staszak-Jirkovsky J, Malliakas CD, Lopes PP, Danilovic N, Kota SS, Chang KC, et al. Design of active and stable Co-Mo-Sx chalcogels as pH-universal catalysts for the hydrogen evolution reaction. Nat Mater. 2016;15(2):197-+.
- 11 Lin CY, Lay CH, Sen B, Chu CY, Kumar G, Chen CC, et al. Fermentative hydrogen production from wastewaters: A review and prognosis. International Journal of Hydrogen Energy. 2012;37(20):15632-42.
- 12 Kirtay E. Recent advances in production of hydrogen from biomass. Energ Convers Manage. 2011;52(4):1778-89.
- 13 Balat H, Kirtay E. Hydrogen from biomass Present scenario and future prospects. International Journal of Hydrogen Energy. 2010;35(14):7416-26.
- 14 Jeremiasse AW, Bergsma J, Kleijn JM, Saakes M, Buisman CJN, Stuart MC, et al. Performance of metal alloys as hydrogen evolution reaction catalysts in a microbial electrolysis cell. International Journal of Hydrogen Energy. 2011;36(17):10482-9.
- 15 Dinh CT, Jain A, de Arquer FPG, De Luna P, Li J, Wang N, et al. Multi-site electrocatalysts for hydrogen evolution in neutral media by destabilization of water molecules. Nat Energy. 2019;4(2):107-14.
- 16 Strmcnik D, Lopes PP, Genorio B, Stamenkovic VR, Markovic NM. Design principles for hydrogen evolution reaction catalyst materials. Nano Energy. 2016;29:29-36.
- 17 Subbaraman R, Tripkovic D, Chang KC, Strmcnik D, Paulikas AP, Hirunsit P, et al. Trends in activity for the water electrolyser reactions on 3d M(Ni,Co,Fe,Mn) hydr(oxy)oxide catalysts. Nat Mater. 2012;11(6):550-7.
- 18 Gong M, Zhou W, Kenney MJ, Kapusta R, Cowley S, Wu YP, et al. Blending Cr2O3 into a NiO-Ni Electrocatalyst for Sustained Water Splitting. Angew Chem Int Edit. 2015;54(41):11989-93.
- 19 Bar-Ziv R, Meiron OE, Bar-Sadan M. Enhancing the catalytic activity of the alkaline hydrogen evolution reaction by tuning the S/Se ratio in the Mo(SxSe₁-x)(2) catalyst. Nanoscale. 2018;10(34):16211-6.
- 20 Gong M, Zhou W, Tsai MC, Zhou JG, Guan MY, Lin MC, et al. Nanoscale nickel oxide/nickel heterostructures for active hydrogen evolution electrocatalysis. Nat Commun. 2014;5.
- 21 Jin HY, Wang J, Su DF, Wei ZZ, Pang ZF, Wang Y. In situ Cobalt-Cobalt Oxide/N-Doped Carbon Hybrids As Superior Bifunctional Electrocatalysts for Hydrogen and Oxygen Evolution. J Am Chem Soc. 2015;137(7):2688-94.
- 22 Wang PT, Zhang X, Zhang J, Wan S, Guo SJ, Lu G, et al. Precise tuning in platinum-nickel/ nickel sulfide interface nanowires for synergistic hydrogen evolution catalysis. Nat Commun. 2017;8.
- 23 Subbaraman R, Tripkovic D, Strmcnik D, Chang KC, Uchimura M, Paulikas AP, et al. Enhancing Hydrogen Evolution Activity in Water Splitting by Tailoring Li+-Ni(OH)(2)-Pt Interfaces. Science. 2011;334(6060):1256-60.
- 24 Yin HJ, Zhao SL, Zhao K, Muqsit A, Tang HJ, Chang L, et al. Ultrathin platinum nanowires grown on single-layered nickel hydroxide with high hydrogen evolution activity. Nat Commun. 2015;6.

- 25 Alexander AM, Hargreaves JSJ. Alternative catalytic materials: carbides, nitrides, phosphides and amorphous boron alloys. Chemical Society Reviews. 2010;39(11):4388-401.
- 26 Xing Z, Liu Q, Asiri AM, Sun X. Closely interconnected network of molybdenum phosphide nanoparticles: a highly efficient electrocatalyst for generating hydrogen from water. Adv Mater. 2014;26(32):5702-7.
- 27 Bai J, Li X, Wang A, Prins R, Wang Y. Hydrodesulfurization of dibenzothiophene and its hydrogenated intermediates over bulk MoP. Journal of Catalysis. 2012;287:161-9.
- 28 Xiao P, Sk MA, Thia L, Ge XM, Lim RJ, Wang JY, et al. Molybdenum phosphide as an efficient electrocatalyst for the hydrogen evolution reaction. Energ Environ Sci. 2014;7(8):2624-9.
- 29 Pu Z, Wei S, Chen Z, Mu S. Flexible molybdenum phosphide nanosheet array electrodes for hydrogen evolution reaction in a wide pH range. Applied Catalysis B: Environmental. 2016;196:193-8.
- 30 Gao S, Liu Y, Li G-D, Guo Y, Zou Y, Zou X. General ureaassisted synthesis of carbon-coated metal phosphide nanoparticles for efficient hydrogen evolution electrocatalysis. Electrochimica Acta. 2016;199:99-107.
- 31 Ammam M. Polyoxometalates: formation, structures, principal properties, main deposition methods and application in sensing. Journal of Materials Chemistry A. 2013;1(21).
- 32 Wang X-D, Xu Y-F, Rao H-S, Xu W-J, Chen H-Y, Zhang W-X, et al. Novel porous molybdenum tungsten phosphide hybrid nanosheets on carbon cloth for efficient hydrogen evolution. Energy Environ Sci. 2016;9(4):1468-75.
- 33 Jiang J, Wang C, Zhang J, Wang W, Zhou X, Pan B, et al. Synthesis of FeP₂/C nanohybrids and their performance for hydrogen evolution reaction. J Mater Chem A. 2015;3(2):499-503.
- Dai HY, Yang HM, Liu X, Jian X, Liang ZH. Electrochemical evaluation of nano-Mg(OH)(2)/graphene as a catalyst for hydrogen evolution in microbial electrolysis cell. Fuel. 2016;174:251-6.
- Kibsgaard J, Jaramillo TF. Molybdenum phosphosulfide: an active, acid-stable, earth-abundant catalyst for the hydrogen evolution reaction. Angew Chem Int Ed Engl. 2014;53(52):14433-7.
- 36 Duan HH, Li DG, Tang Y, He Y, Ji SF, Wang RY, et al. High-Performance Rh2P Electrocatalyst for Efficient Water Splitting. J Am Chem Soc. 2017;139(15):5494-502.
- 37 Danilovic N, Subbaraman R, Strmcnik D, Chang KC, Paulikas AP, Stamenkovic VR, et al. Enhancing the Alkaline Hydrogen Evolution Reaction Activity through the Bifunctionality of Ni(OH)2/Metal Catalysts. Angew Chem Int Edit. 2012;51(50):12495-8.
- 38 Caban-Acevedo M, Stone ML, Schmidt JR, Thomas JG, Ding Q, Chang HC, et al. Efficient hydrogen evolution catalysis using ternary pyrite-type cobalt phosphosulphide. Nat Mater. 2015;14(12):1245-51.
- 39 Merki D, Vrubel H, Rovelli L, Fierro S, Hu XL. Fe, Co, and Ni ions promote the catalytic activity of amorphous molybdenum sulfide films for hydrogen evolution. Chem Sci. 2012;3(8):2515-25.

Table of Content:

